

Article

Segregation of P and S Impurities to A Σ 9 Grain Boundary in Cu

Cláudio M. Lousada * and Pavel A. Korzhavii 

Department of Materials Science and Engineering, KTH Royal Institute of Technology, SE-100 44 Stockholm, Sweden; pavelk@kth.se

* Correspondence: cmlp@kth.se; Tel.: +46-879-06-252

Received: 27 July 2020; Accepted: 9 October 2020; Published: 13 October 2020



Abstract: The segregation of P and S to grain boundaries (GBs) in fcc Cu has implications in diverse physical-chemical properties of the material and this can be of particular high relevance when the material is employed in high performance applications. Here, we studied the segregation of P and S to the symmetric tilt Σ 9 (221) [110], 38.9° GB of fcc Cu. This GB is characterized by a variety of segregation sites within and near the GB plane, with considerable differences in both atomic site volume and coordination number and geometry. We found that the segregation energies of P and S vary considerably both with distance from the GB plane and sites within the GB plane. The segregation energy is significantly large at the GB plane but drops to almost zero at a distance of only ≈ 3.5 Å from this. Additionally, for each impurity there are considerable variations in energy (up to 0.6 eV) between segregation sites in the GB plane. These variations have origins both in differences in coordination number and atomic site volume with the effect of coordination number dominating. For sites with the same coordination number, up to a certain atomic site volume, a larger atomic site volume leads to a stronger segregation. After that limit in volume has been reached, a larger volume leads to weaker segregation. The fact that the segregation energy varies with such magnitude within the Σ 9 GB plane may have implications in the accumulation of these impurities at these GBs in the material. Because of this, atomic-scale variations of concentration of P and S are expected to occur at the Σ 9 GB center and in other GBs with similar features.

Keywords: grain boundaries; segregation; copper; density functional theory; sigma 9; Σ 9

1. Introduction

The binding energy of substitutional and interstitial impurities to grain boundaries (GBs) is highly dependent of the local structure of the GBs [1,2]. This is because at many GB the local atomic environment differs considerably when compared to the bulk [3]. These features have an important direct impact on several local properties of the material at the GBs, such as segregation of impurities, defect mobility and grain boundary sink efficiency [1,4,5]. For some materials, such local GB features can affect the microcrystallinity [6] and other global properties, such as creep [7], plasticity, strength and can also affect hydrogen embrittlement and stress corrosion cracking mechanisms [8–10]. These phenomena have additional relevance when the material is used in high performance applications, such as in long-term repositories for spent nuclear fuel.

For a specific GB, the local atomic environment can also vary considerably. This happens both within the GB plane and along the direction perpendicular to the GB plane. We have shown previously that for fcc Cu the Σ 5 and Σ 11 GBs can increase the strength of the segregation of substitutional impurities at certain atomic sites while the Σ 3 GB has no ability to trigger the segregation of impurities [7]. The dominating effect is the volume expansion at certain GB sites of the Σ 5 and Σ 11 and because the

$\Sigma 3$ has no sites with considerable volume expansion, the segregation of impurities from the bulk is not favorable [1,7].

For oxygen free Cu (Cu-OF) it has been shown that the presence of phosphorus improves the creep properties at near ambient temperatures [11,12]. The underlying mechanisms involve the formation of cavities and the presence of P is thought to largely influence those mechanisms [13,14]. Previous studies suggested that the presence of S could also affect those mechanisms but a recent study did not find convincing correlations between the amounts of S present in the GBs and the creep ductility of Cu [13]. In previous studies it was also found that S segregates at Cu GBs [2,15], and the effects of the presence of S on the mechanisms of segregation of P at those GBs are currently not understood. Because these two impurities share many similarities in terms of segregation mechanisms and energies [7], it is important to understand their tendencies for segregation at GBs in Cu in order to have a more detailed picture of the local GB chemistry, because this can affect the global, macroscopic properties of the material. Our previous investigations on the segregation of P and S at low index symmetric tilt GBs of Cu— $\Sigma 3$, $\Sigma 5$ and $\Sigma 11$ —have shown a large variation in the segregation energies (ΔE_{seg}) for these elements both as a function of GB type and as a function of the distance from the GB plane [7]. However, the $\Sigma 3$, $\Sigma 5$ and $\Sigma 11$ GBs have as a common feature, the fact that within their GB planes, the coordination, geometry and local volume for copper atoms and interstitial sites is fairly homogeneous and considerable variations in these features occur only as a function of distance from the GB plane [1]. In order to understand if the ΔE_{seg} can also vary considerably within GB planes it is important to study other GBs with a more diverse local atomic environment within GB plane. The $\Sigma 9$ GB has a variety of atomic positions within the GB plane where half of the GB resembles the $\Sigma 3$ and the remaining half is dominated by a cavity with a larger volume expansion than the $\Sigma 5$ [16]. Because the $\Sigma 9$ GB can occur with considerable frequency in Cu [16–18], the goal of this study is to investigate the segregation of P and S to the $\Sigma 9$ GB with density functional theory (DFT) calculations and compare how it differs from the previously studied GBs. We found large variations in ΔE_{seg} obtained for $\Sigma 9$ for both P and S within the GB plane, which is a unique feature among the $\Sigma 9$, $\Sigma 3$, $\Sigma 5$ and $\Sigma 11$ GBs. Similarly to the other GBs previously studied, ΔE_{seg} varies significantly with distance from the GB plane. Overall, we found that for the $\Sigma 9$ GB, the segregation tendency for the substitutional impurities P and S has larger variations than for the $\Sigma 3$, $\Sigma 5$ and $\Sigma 11$ GBs. This happens both within the GB plane and as a function of distance from the GB plane.

2. Materials and Methods

Density functional theory (DFT) calculations of the segregation or absorption of S and P to the $\Sigma 9$ GB of fcc Cu were performed with the Vienna *ab initio* simulation package (VASP 5.4.1) [19] with the Perdew–Burke–Ernzerhof [20] (PBE) exchange–correlation functional with pseudopotentials of the projector augmented wave [21,22] (PAW) type. The PBE functional showed good accuracy for describing the interactions between p-block elements with the bulk and surfaces of Cu [2,23–26]. For all calculations, a plane wave cutoff of 460 eV and a k-point mesh of $(7 \times 9 \times 3)$ in the Monkhorst–Pack sampling scheme were employed [27]. The energies herein reported are electronic energies at 0 K which allow accurate comparisons between binding energies at sites with similar chemical environment in the solid [28–30]. The segregation energy (ΔE_{seg}) of an element X at a GB site is defined as

$$\Delta E_{\text{seg}} = E_{(X_{\text{GB}})} - E_{(X_{\text{Bulk}})} \quad (1)$$

where $E_{(nX_{\text{GB}})}$ is the energy of a supercell of Cu containing a GB model with the dopant X placed in a substitutional site at the GB plane or in its close-vicinity, and $E_{(nX_{\text{Bulk}})}$ is the reference energy of the same supercell with the dopant placed far from the GB plane at a bulk site. A more negative value for ΔE_{seg} implies stronger bonding and a value equal to zero implies no preference for bonding to the respective site compared to the bulk. The GB energy is here defined as

$$\gamma_{\text{GB}} = (E_{\text{GB}} - E_{\text{bulk}})/2A \quad (2)$$

where the electronic energies are: E_{GB} , the energy of the supercell that contains the GB; E_{bulk} , the total energy of a supercell of Cu single crystal that contains the same number of atoms as those present in the supercell used for modelling the GB and A , area of the GB in the supercell. The quantity is divided by two to account for the fact that there are two identical GBs in the supercell. Lower values of γ_{GB} imply stronger cohesive bonding between the two grains. The GB model $\Sigma 9$ ($2\bar{2}\bar{1}$) [110], 38.9° consisting of a supercell with dimensions: $x = 7.67 \text{ \AA}$, $y = 5.11 \text{ \AA}$ and $z = 21.13 \text{ \AA}$ is shown in Figure 1.

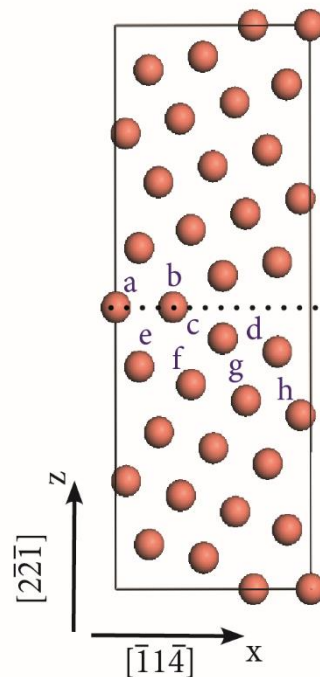


Figure 1. Geometry optimized $\Sigma 9$ grain boundaries (GB) employed to study the segregation of P and S. Atomic sites (a to h) where the segregation of P and S as substitutional impurities was studied.

We have chosen this GB because it occurs frequently in fcc Cu [16–18] and it has a geometry with a diverse openness due to sites with different coordination numbers and local volume at the GB plane. In a previous work we have shown that the volume expansion is a key parameter for driving the segregation of dopants to GBs [1,7]. The GB model of Figure 1 was constructed using the coincidence-site lattice (CSL) method and a periodic supercell that contains two oppositely oriented $\Sigma 9$ GBs. The CSL allows the accurate construction of periodic GB models of single crystals for GBs that have a high density of coincidence sites at the GB plane [31,32]. After the construction of the model with the CLS method, a first optimization of the GB supercell was performed. In this optimization step the supercell containing the GB was relaxed along the $[2\bar{2}\bar{1}]$ direction. After this optimization was completed, an optimization of the internal coordinates of all atoms was carried out. Additional optimizations of the supercell and of the internal coordinates were iteratively carried out until the optimized geometry shown in Figure 1 was found. The self-consistent field (SCF) electronic energies were considered converged when their change between two cycles was smaller than $1 \times 10^{-5} \text{ eV}$ and the forces acting on each of the atoms smaller than $0.002 \text{ eV} \cdot \text{\AA}^{-1}$ for the ionic relaxations and additionally zero Pulay stress for the supercell optimization. For the determination of the segregation energies, the internal coordinates of all atoms of the supercell were optimized. The GB model employed, shown in Figure 1, has been optimized and then benchmarked against a supercell of single crystal fcc Cu. In the GB model, the distance from the GB plane to a parallel plane where we consider that the binding energy of a dopant is equal to that of bulk Cu was validated by comparison with the case where the dopant is at a substitutional site in a supercell of single crystal fcc Cu with symmetry $(3 \times 3 \times 3)$

containing 108 Cu-atoms. The difference between both values is in the order of 0.003 eV. This value is considered as the limit of error of the computational method.

The coordination numbers and atomic site volumes were determined using Voronoi tessellation of the supercell. The volume expansion (%) of a given atomic site is here defined relative to the volume at the bulk fcc site as

$$V_e = \frac{(V_s - V_b) \times 100}{V_b} \quad (3)$$

where V_e is the volume expansion (%), V_s is the volume of the atomic site s and V_b is the volume at the bulk fcc site.

3. Results and Discussion

The obtained GB energy for the $\Sigma 9$ GB model shown in Figure 1 is 689 mJ/m² which is in good agreement with the literature data: 1200 mJ/m², 859 mJ/m² and 850 mJ/m² [16,33,34]. The study of the segregation of P and S as substitutional impurities was done by sequentially placing one dopant at a time on the sites labelled in Figure 1 to replace the corresponding Cu atom. The obtained ΔE_{seg} are given in Table 1 and the plot of the ΔE_{seg} as a function of the distance from the GB plane for both P and S are shown in Figure 2.

Table 1. Segregation energies ΔE_{seg} (eV) for P and S for the atomic sites labelled in Figure 1, the respective distances (d) from the GB plane, coordination number of the site and volume expansion relative to the fcc single crystal (%).

Atomic Position	Impurity		z Coordinate (fractional)	z Coordinate (Å)	d (Å)	Coordination Number	Volume Expansion (%)
	P (ΔE_{seg})	S (ΔE_{seg})					
a	−0.653	−0.724	0.500	10.853	0.000	10	2.3
b	0.009	−0.335	0.500	10.853	0.000	14	14.0
c	−0.493	−0.655	0.443	9.675	1.248	10	6.7
d	−0.274	−0.384	0.421	9.167	1.716	11	6.6
e	−0.276	−0.562	0.392	8.636	2.360	12	5.5
f	−0.243	−0.274	0.363	7.956	2.972	12	0.5
g	0.065	0.000	0.340	7.343	3.488	12	−0.9
h	0.013	0.000	0.315	6.808	4.015	12	0.8

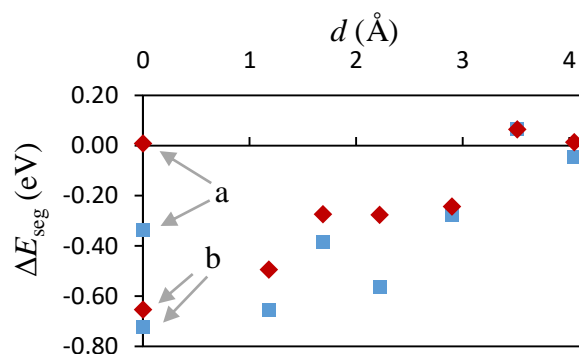


Figure 2. Segregation energies ΔE_{seg} (eV) for P and S to the $\Sigma 9$ GB as a function of distance from the GB center (d) (Å). S (■), P (◆). The labels a and b represent the data points for sites a and b.

The ΔE_{seg} vary significantly as a function of the distance from the GB center due to changes in coordination number and volume expansion, as will be shown below. This is in line with previous findings for $\Sigma 3$, $\Sigma 5$ and $\Sigma 11$ GBs [7]. From these three GBs, the $\Sigma 5$ is that where P and S have the largest ΔE_{seg} and additionally, from these three GBs the change in ΔE_{seg} as a function of d is largest for $\Sigma 5$. For the current case of the $\Sigma 9$ GB, it can be seen however that the dependency of ΔE_{seg} on d is even stronger than what was previously found for $\Sigma 5$ [7]. While for the $\Sigma 9$ the ΔE_{seg} is of considerable magnitude in the GB plane for sites a and c, it can be seen that already at a distance of only ≈ 3.5 Å there is no driving force for segregation because $\Delta E_{\text{seg}} = 0$. Additionally, a unique feature of the $\Sigma 9$ GB is that at the GB plane there is a considerable difference in ΔE_{seg} , as shown by the values obtained for the sites a and b.

The difference between ΔE_{seg} for sites a and b is of around 0.6 eV for P and of around 0.4 eV for S, although both sites lay in the GB plane. This has not been previously observed for the $\Sigma 3$, $\Sigma 5$ and $\Sigma 11$ GBs. As can be seen in the data of Table 1, site b has a considerably larger volume expansion than site a, simultaneously the coordination number for site b is of 14 when compared to a coordination number of 10 for site a. The coordination number and volume expansion for sites a and c show that even though site c has a larger volume expansion than site a, it leads to similarly large values of ΔE_{seg} for both P and S which indicates that the same coordination number for site c as for site a is the factor that has the largest effect in the ΔE_{seg} . A plot of the coordination number of the different sites vs. the respective ΔE_{seg} are shown in Figure 3.

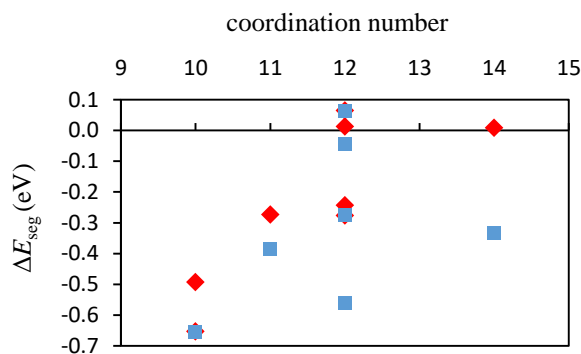


Figure 3. Segregation energies ΔE_{seg} (eV) for P and S to the $\Sigma 9$ GB as a function of the coordination number of the segregation site. S (■), P (◆).

In this figure it is visible that lower coordination numbers lead to a larger magnitude of ΔE_{seg} . The magnitude of ΔE_{seg} decreases with increasing coordination number up to a coordination number of 12 which is the coordination number of the fcc single crystal. For the sites with coordination number 12, the differences in ΔE_{seg} are due to effects of volume expansion. For the sites with coordination number 12, larger volume expansion leads to larger magnitude of ΔE_{seg} and consequently stronger segregation of impurities. This effect has been previously observed for a single crystal of fcc Cu [1]. It can be seen additionally that the atomic sites c and d produce considerably different values of ΔE_{seg} . Both sites have the same volume expansion, but site c has a coordination number of 10 while site d has a coordination number of 11. This highlights again the importance of the coordination number in driving the segregation of impurities. It has been observed previously that the volume expansion and the coordination: bond number and geometry, affect the ΔE_{seg} of impurities at the GBs and at the bulk [1,7]. Moving away from the GB plane towards the bulk decreases the volume expansion which together with an increase in the coordination number causes the ΔE_{seg} to become smaller.

The importance of rationalizing the ΔE_{seg} with GB structure can be seen in the non-linear effects of the changes in coordination number and volume on the values of ΔE_{seg} . For example, sites a and b both have different coordination numbers and atomic site volumes. Site b has a considerably higher coordination number (CN = 14) and volume expansion (14.0%) when compared to CN = 10 and

volume expansion of 2% for site a, respectively. Site a is a near neighbor to the large cavity located at the GB center which leads to a lower coordination number and a not too large volume expansion. This results in an additional driving force for bonding the impurities to site a, which is reflected in the ΔE_{seg} obtained for this site when compared to site b. A similar phenomenon occurs for sites c and d. Site c is located near the central GB cavity and has a volume expansion of 6.7% when compared to the bulk. The volume expansion at site d is similar, 6.6%, but the coordination number of site c is 10 while that of site d is 11. This leads to a smaller magnitude of ΔE_{seg} for site d when compared to site c. These effects that determine the ΔE_{seg} are the result of the balance between volume expansion and coordination. The values of ΔE_{seg} for sites a and c are larger than for sites b and d, respectively, because in the former pair of sites the coordination numbers are smaller. The effect of the volume expansion can be clearly seen when comparing sites with the same coordination number. The volume expansion can have a favorable effect in driving the segregation if the volume expansion is within the limits that favor the bonding of the impurities with neighboring Cu atoms.

Both P and S have similar ΔE_{seg} and the variation in the values with d and coordination number follows a similar trend for both cases. For the same sites, S tends to have a larger magnitude of ΔE_{seg} than P and we can conclude that if both impurities compete for the same atomic site the segregation of S is favored over that of P. Overall, we also found that the coordinates of the Cu atoms that are first neighbors to the impurities suffer slight changes due to the presence of the impurities. The Cu-P or Cu-S bond distances became shorter by up to 0.1 Å when compared to the Cu-Cu distances for the same atomic positions without the presence of the impurities. The occurrence of such contractions, even if small, is also favored by volume expansion and lower coordination number at those sites.

4. Conclusions

The $\Sigma 9$ grain boundary (GB) has a varied coordination environment and contains atomic sites with considerable differences in atomic site volume within the GB plane. Among the low index GBs this is a unique feature and provides good ground for understanding the geometric effects that are at the origin of the differences in segregation energies for different GB sites. Our data show that the segregation energies of the substitutional impurities P and S vary considerably with distance from the GB plane. The distance from the GB center in turn affects considerably the coordination number and volume expansion of the sites. While the segregation energies are considerably large at the GB, at only ≈ 3.5 Å the segregation is not favorable. At the GB plane there are significant differences in the segregation energies for each impurity with differences in the order of ≈ 0.6 eV. At the origin of these effects is a combination of coordination number and volume expansion. We find that the coordination number is a dominating effect but for sites with the same coordination number a larger volume expansion leads to a stronger segregation.

The large differences in segregation energies at the GB plane for the $\Sigma 9$ GB is a unique feature among lower index symmetric tilt GBs where the segregation of these impurities has been previously studied: $\Sigma 3$, $\Sigma 5$ and $\Sigma 11$. The fact that the segregation energies vary with such magnitudes within the $\Sigma 9$ GB plane may have implications in the accumulation of these impurities at GBs in the material. In this sense, atomic-scale variations of concentration of these impurities are expected to occur at the $\Sigma 9$ GB and other GBs with similar features.

Author Contributions: Conceptualization, C.M.L. and P.A.K.; computations C.M.L., writing—original draft preparation, C.M.L.; writing—review and editing, C.M.L. and P.A.K. All authors have read and agreed to the published version of the manuscript.

Funding: Financial support from the Swedish Nuclear Fuel and Waste Management Company (SKB) is gratefully acknowledged. The computations were performed on resources provided by the Swedish National Infrastructure for Computing (SNIC) at the PDC Center for High Performance Computing at the KTH—Royal Institute of Technology, Stockholm, partially funded by the Swedish Research Council through grant agreement no. 2016-07213.

Conflicts of Interest: The authors declare no conflict of interest.

References

1. Lousada, C.M.; Korzhavyi, P.A. Hydrogen sorption capacity of crystal lattice defects and low Miller index surfaces of copper. *J. Mater. Sci.* **2020**, *55*, 6623–6636. [[CrossRef](#)]
2. Li, Y.; Korzhavyi, P.A.; Sandström, R.; Lilja, C. Impurity effects on the grain boundary cohesion in copper. *Phys. Rev. Mater.* **2017**, *1*, 070602. [[CrossRef](#)]
3. Amelinckx, S.; Dekeyser, W. The Structure and Properties of Grain Boundaries. In *Solid State Physics*; Seitz, F., Turnbull, D., Eds.; Academic Press: New York, NY, USA, 1959; Volume 8, pp. 325–499.
4. Uberuaga, B.P.; Vernon, L.J.; Martinez, E.; Voter, A.F. The relationship between grain boundary structure, defect mobility and grain boundary sink efficiency. *Sci. Rep.* **2015**, *5*, 9095. [[CrossRef](#)] [[PubMed](#)]
5. Herbig, M.; Raabe, D. Atomic scale quantification of grain boundary segregation in nanocrystalline material. *Phys. Rev. Lett.* **2014**, *112*, 126103. [[CrossRef](#)] [[PubMed](#)]
6. Mishin, Y.; Asta, M.; Li, J. Atomistic modeling of interfaces and their impact on microstructure and properties. *Acta Mater.* **2010**, *58*, 1117–1151. [[CrossRef](#)]
7. Sandström, R.; Lousada, C.M. The role of binding energies for phosphorus at grain boundaries in copper. *J. Nucl. Mater.* **2020**. (under review).
8. Rupert, T.J.; Trelewicz, J.R.; Schuh, C.A. Grain boundary relaxation strengthening of nanocrystalline Ni–W alloys. *J. Mater. Res.* **2012**, *27*, 1285–1294. [[CrossRef](#)]
9. Rogers, H.C. Hydrogen Embrittlement of Metals. *Science* **1968**, *159*, 1057–1064. [[CrossRef](#)]
10. King, A.; Johnson, G.; Engelberg, D.; Ludwig, W.; Marrow, J. Observations of intergranular stress corrosion cracking in a grain-mapped polycrystal. *Science* **2008**, *321*, 382–385. [[CrossRef](#)]
11. Korzhavyi, P.A.; Sandström, R. First-principles evaluation of the effect of alloying elements on the lattice parameter of a 23Cr25NiWCuCo austenitic stainless steel to model solid solution hardening contribution to the creep strength. *Mater. Sci. Eng. A* **2015**, *626*, 213–219. [[CrossRef](#)]
12. Sandström, R.; Wu, R. Influence of phosphorus on the creep ductility of copper. *J. Nucl. Mater.* **2013**, *441*, 364–371. [[CrossRef](#)]
13. Henderson, P.J.; Sandström, R. Low temperature creep ductility of OFHC copper. *Mater. Sci. Eng. A* **1998**, *246*, 143–150. [[CrossRef](#)]
14. Sandström, R.; Wu, R. *Origin of the Extra Low Creep Ductility of Copper without Phosphorus*; Swedish Nuclear Waste Management Company Report TR-07-02; Swedish Nuclear Waste Management Company: Stockholm, Sweden, 2007.
15. Bowyer, W.H. *The Effects of Impurities on the Properties of OFP Copper Specified for the Copper Iron Canister*; SKI Report 99:44; SKI: Stockholm, Sweden, 1999.
16. Hallberg, H.; Olsson, P.A.T. Investigation of microstructure evolution during self-annealing in thin Cu films by combining mesoscale level set and ab initio modeling. *J. Mech. Phys. Solids* **2016**, *90*, 160–178. [[CrossRef](#)]
17. Mishin, O.V.; Gertsman, V.Y.; Gottstein, G. Distributions of orientations and misorientations in hot-rolled copper. *Mater. Charact.* **1997**, *38*, 39–48. [[CrossRef](#)]
18. Korolev, V.V.; Kucherinenko, Y.V.; Makarevich, A.M.; Straumal, B.B.; Protsenko, P.V. Statistics of GB misorientations in 2D polycrystalline copper foil. *Mater. Lett.* **2017**, *196*, 377–380. [[CrossRef](#)]
19. Kresse, G.; Furthmüller, J. Efficient iterative schemes for ab initio total-energy calculations using a plane-wave basis set. *Phys. Rev. B* **1996**, *54*, 11169–11186.
20. Perdew, J.P.; Burke, K.; Ernzerhof, M. Generalized Gradient Approximation Made Simple. *Phys. Rev. Lett.* **1996**, *77*, 3865–3868, Erratum in **1997**, *78*, 1396–1396. [[CrossRef](#)] [[PubMed](#)]
21. Blöchl, P.E. Projector augmented-wave method. *Phys. Rev. B* **1994**, *50*, 17953–17979. [[CrossRef](#)] [[PubMed](#)]
22. Kresse, G.; Joubert, D. From ultrasoft pseudopotentials to the projector augmented-wave method. *Phys. Rev. B* **1999**, *59*, 1758–1775. [[CrossRef](#)]
23. Lousada, C.M.; Johansson, A.J.; Korzhavyi, P.A. Molecular and dissociative adsorption of water and hydrogen sulfide at perfect and defective Cu(110) surfaces. *Phys. Chem. Chem. Phys.* **2017**, *19*, 8111–8120. [[CrossRef](#)]
24. Lousada, C.M.; Johansson, A.J.; Korzhavyi, P.A. Molecular and dissociative adsorption of water at a defective Cu(110) surface. *Surf. Sci.* **2017**, *658*, 1–8. [[CrossRef](#)]
25. Lousada, C.M.; Johansson, A.J.; Korzhavyi, P.A. Adsorption of Hydrogen Sulfide, Hydrosulfide and Sulfide at Cu(110)—Polarizability and Cooperativity Effects. First Stages of Formation of a Sulfide Layer. *ChemPhysChem* **2018**, *19*, 2159–2168. [[CrossRef](#)] [[PubMed](#)]

26. Lousada, C.M.; Johansson, A.J.; Korzhavyi, P.A. Thermodynamics of H₂O Splitting and H₂ Formation at the Cu(110)–Water Interface. *J. Phys. Chem. C* **2015**, *119*, 14102–14113. [[CrossRef](#)]
27. Methfessel, M.; Paxton, A.T. High-precision sampling for Brillouin-zone integration in metals. *Phys. Rev. B* **1989**, *40*, 3616–3621. [[CrossRef](#)]
28. You, Y.-W.; Kong, X.-S.; Wu, X.-B.; Xu, Y.-C.; Fang, Q.F.; Chen, J.L.; Luo, G.-N.; Liu, C.S.; Pan, B.C.; Wang, Z. Dissolving, trapping and detrapping mechanisms of hydrogen in bcc and fcc transition metals. *AIP Adv.* **2013**, *3*, 012118. [[CrossRef](#)]
29. Lousada, C.M.; Sophonrat, N.; Yang, W. Mechanisms of Formation of H, HO, and Water and of Water Desorption in the Early Stages of Cellulose Pyrolysis. *J. Phys. Chem. C* **2018**, *122*, 12168–12176. [[CrossRef](#)]
30. Heinola, K.; Ahlgren, T.; Nordlund, K.; Keinonen, J. Hydrogen interaction with point defects in tungsten. *Phys. Rev. B* **2010**, *82*, 094102. [[CrossRef](#)]
31. Randle, V. The coincidence site lattice and the ‘sigma enigma’. *Mater. Charact.* **2001**, *47*, 411–416. [[CrossRef](#)]
32. Fortes, M.A. Coincidence Site Lattices. *Phys. Status Solidi (b)* **1972**, *54*, 311–319. [[CrossRef](#)]
33. Wan, L.; Wang, S. Shear response of the $\Sigma 9 \langle 110 \rangle \{221\}$ symmetric tilt grain boundary in fcc metals studied by atomistic simulation methods. *Phys. Rev. B* **2010**, *82*, 214112. [[CrossRef](#)]
34. Tschopp, M.A.; Coleman, S.P.; McDowell, D.L. Symmetric and asymmetric tilt grain boundary structure and energy in Cu and Al (and transferability to other fcc metals). *Integr. Mater. Manuf. Innov.* **2015**, *4*, 176–189. [[CrossRef](#)]



© 2020 by the authors. Licensee MDPI, Basel, Switzerland. This article is an open access article distributed under the terms and conditions of the Creative Commons Attribution (CC BY) license (<http://creativecommons.org/licenses/by/4.0/>).